



Evolution of amorphous carbon across densities: An inferential study

Bishal Bhattarai^{a,*}, Anup Pandey^b, D.A. Drabold^{c,**}

^a Department of Physics and Astronomy, Condensed Matter and Surface Science Program (CMSS), Ohio University, Athens, OH, 45701, USA

^b Neutron Scattering Division, Oak Ridge National Laboratory, Oak Ridge, TN, 37831, USA

^c Department of Physics and Astronomy, Nanoscale and Quantum Phenomena Institute (NQPI), Ohio University, Athens, OH, 45701, USA

ARTICLE INFO

Article history:

Received 28 September 2017

Received in revised form

26 January 2018

Accepted 31 January 2018

Available online 6 February 2018

Keywords:

ab initio

Reverse monte carlo

Inverse modeling

Amorphous carbon

Phonons

ABSTRACT

In this paper, we offer large and realistic models of amorphous carbon spanning densities from 0.95 g/cm^3 to 3.5 g/cm^3 . The models are *designed* to agree as closely as possible with experimental diffraction data while simultaneously attaining a local energy minimum of a density functional Hamiltonian. The structure varies dramatically from interconnected wrapped and defective sp^2 sheets at 0.95 g/cm^3 to a nearly perfect tetrahedral topology at 3.5 g/cm^3 . Force Enhanced Atomic Refinement (FEAR) was used and is shown here to be advantageous relative to conventional *ab initio* melt quench methods. We thoroughly characterize our models by computing structural, electronic and vibrational properties. The vibrational density of states of the 0.95 g/cm^3 model is strikingly similar to monolayer amorphous graphene. Our sp^2/sp^3 ratios are close to experimental predictions where available.

© 2018 Elsevier Ltd. All rights reserved.

1. Introduction

Amorphous carbon (a-Carbon) has numerous applications [1–3]. a-Carbon with high sp^3 content [4] is also referred to as Diamond like Carbon (DLC). DLC films are crucial in industry, as it is widely used for coating for optical windows, hard drives and other electromechanical devices [1,5]. Meanwhile, porous carbons are used in several applications like gas storage, filtration, energy and steel production [5,6]. Experimentally, amorphous carbon ranging from low to high density and is produced by deposition from filtered energy ion beams [7–9]. Further, it has been observed with diffraction experiments that a-Carbon exists with various bonding environments (sp , sp^2 and sp^3) depending upon the sample density. A lack of long-range order, different bonding environments and presence of porosity in a-Carbon [6], imposes a challenge for condensed matter theorists.

A logical approach for determining structure is to use experiment to infer or “invert” that structure. This is accepted practice for crystals, even those with extremely large unit cells. For amorphous materials, a unique inversion is impossible because of the smooth structure factors and pair-correlation functions. A venerable

alternative, the method of “melt quenching” (MQ) is limited by fast quenching rates and ignores *a priori* experimental information in the process of model formation [10]. In the context of a-Carbon, classical simulations *via* MQ is significantly dependent upon the choice of interatomic potentials [5]. We bridge the divide between these approaches in this paper.

For proper context we note that inverse modeling is experimentally driven and usually utilizes a Reverse Monte Carlo (RMC) [11–15] method. RMC produces a model matching experiments (most often scattering experiments sensitive to pair-correlations). It is relatively easy to implement and is computationally inexpensive. It is a very sensible idea, but RMC can yield models with qualitatively incorrect coordination and/or chemical order, because the method in its usual form includes no *a priori* information about chemistry [16,17]. To resolve this trouble, different constraints have been included in the RMC refinement process such as: multiple scattering data [18–20], bond-angle constraints [21], coordination constraints [13] and so on, which can be quite effective in producing desired results [16]. The concern about invoking constraints is that this introduces a researcher's bias (that is, information not directly from an experiment) into the modeling, and contradicts the underlying concept of “allowing the data to speak for itself”. Various approaches [22–26] mix energy minimization with RMC-type schemes [5,27–32].

We have implemented our Force Enhanced Atomic Refinement (FEAR) [24–26] method in a-Carbon. FEAR offers the logical

* Corresponding author.

** Corresponding author.

E-mail addresses: bb248213@ohio.edu (B. Bhattarai), ap439111@ohio.edu (A. Pandey), drabold@ohio.edu (D.A. Drabold).

advantage of using *a priori* knowledge, but within an *ab initio* simulation framework. Its ability to predict accurate structure with correct chemical composition, starting from a *random* structure without any constraints has been a feature of this approach. We have used FEAR with state of the art *ab initio* interactions for our calculations. FEAR has been tested in several materials, it is a robust and efficient method to model different amorphous systems [24,25].

In this paper, we present a series of models of amorphous Carbon at various densities using the same approach for all. We systematically report the dependence of observables on the density. The paper is organized as follows, In section 2 we discuss the computational methodology. In section 3, we report our models and the methods of preparation. Section 4, mainly focuses on the structural properties of the models and comparisons to experiments. Section 5 is devoted to the electronic properties of the system. Section 6 we describe the vibrational properties of these carbons. In section 7, we summarize our findings and discuss the effectiveness of our approach by comparing it to the other known results.

2. Methodology

We have prepared four models of a-Carbon with 648 atoms at densities 3.50 g/cm^3 , 2.99 g/cm^3 , 2.44 g/cm^3 and 0.951 g/cm^3 using FEAR. In FEAR, we begin with *randomly* chosen coordinates which are subjected to partial structural refinement with *M* accepted RMC steps and partial relaxations with the conjugate gradient (CG) method for *N* relaxation steps.¹ This cycle is repeated until the model is fully converged (fitting the data and at the same time, sitting at a suitable minimum of the DFT interactions) [24,25]. To our knowledge, these are the largest *ab initio* models offered to date for a-Carbon.

The relaxation step was performed with a single- ζ basis, periodic boundary conditions and Harris functional at constant volume using SIESTA.² As an additional check of our models, we have relaxed the converged models using the *ab initio* package VASP [34] with plane wave basis [34], $\Gamma(k=0)$, plane-wave cutoff of 400 eV and an energy convergence tolerance of 10^{-4} eV. To compare and contrast, we have also prepared *ab initio* based MQ models. We have prepared three models (160 atom) each using SIESTA (LDA, Harris functional) and VASP (LDA, self-consistency) [35,36].

3. Models

The starting random configuration is fitted to appropriate experimental data with RMCProfile.^{3,4} After every ~ 100 accepted RMC moves [24–26], the total energy and forces were evaluated (using a single force call) and the atoms were moved along the gradient to reduce the total energy. We have chosen a maximum RMC step size of 0.25 Å–0.375 Å, a minimum approach of 1.05 Å–1.20 Å, with a fixed spacing of 0.02 Å and 0.04 – 0.085 weight of the experimental data. Meanwhile, CG relaxation is carried out using SIESTA.

In the meantime, we implemented MQ calculations with random coordinates, which were equilibrated at 7000 K, then cooled to 300 K, further equilibrated at 300 K and finally relaxed using CG method. This process employed a time step of 1.0 fs for a

total simulation time of 26 ps. We have also prepared a self-consistent MQ model using VASP. These models were started from random, then heated to 8000 K, equilibrated at 8000 K, cooled to 300 K and finally relaxed with CG method. A time step of 1.5 fs was used for total time of 24 ps.

These models will hereafter be identified as (F648, S160 and V160). The assigned nomenclature indicates: method of preparation (FEAR-SIESTA-VASP) and number of atoms in the cell of each model. We have used our previous VASP prepared model (V72 at 0.92 g/cm^3) [38] to compare the result of our lowest density model. Our models are summarized in Table 1.

4. Structural properties

Structurally, amorphous carbon at density 3.50 g/cm^3 is diamond-like, (sp^3) whereas near graphitic density 2.27 g/cm^3 , it is mostly sp^2 bonded and at even lower densities ($< 2.0 \text{ g/cm}^3$) we observe a few sp conformations juxtaposed with sp^2 bonded carbon structures [43]. This evolution of bonding with density is shown in Fig. 1. We have assigned different color codes (*via*. Jmol³) for varying coordinations. Our sp^2/sp^3 ratios are close to experimental findings [44,45]. In Fig. 2, we show a comparison of experimental static structure factor $S(Q)$ and radial distribution function (RDF, $g(r)$) with our FEAR models.

At density 3.50 g/cm^3 , we have used a Wooten-Weaire-Winer (WWW) [39] model as our input diffraction data, as no experimental data is available for this density. The WWW model is obtained with a bond-switching-algorithm [46] yielding an idealized (100 % sp^3) bonded network. These models have had many fruitful applications to tetrahedral amorphous systems and beyond [47]. We obtained close agreement for both $S(Q)$ and $g(r)$ with the WWW model, and we found 96 % sp^3 content in our model (Table 1). In contrast, earlier finding [48] report a lower concentration of sp^3 at this density.

We have used experimental diffraction data for the next three calculations. At a density 2.99 g/cm^3 , we employed the neutron diffraction data of Gilkes et al. [40] which is estimated to have 84% sp^3 bonding and a mean coordination-number $n = 3.84$. Our obtained $S(Q)$ and $g(r)$ are in an excellent agreement with experiment and we reproduce 82.70 % sp^3 bonding with mean coordination $n = 3.83$. Similarly, at density 2.44 g/cm^3 , we have used experimental diffraction data of Li and Lannin [41] as our RMC input. We obtain pleasing agreement with the experimental diffraction data ($S(Q)$ and $g(r)$) while some deviations are seen in MQ models. These results for densities (2.99 g/cm^3 and 2.44 g/cm^3) are in better agreement with the experiment compared to some earlier work [6,43,48].

Finally, at low density, our models reveal the presence of voids. For a density lower than graphite (2.26 g/cm^3) the system is comprised mostly of sp^2 carbon, interconnected with a small fraction of sp^3 sites [49]. A notable amount of sp bonded carbon is also seen at these densities [3]. Amorphous carbon at this density is also known as glassy carbon, a bit of a misnomer as the materials are not conventional glasses. The uncertainty of density, structure and significant H-content makes it difficult to study glassy carbons [9,13,17,50,51]. Most calculations include strong assumptions, such as building in perfect hexagonal graphitic or graphene sheets, coordination restrictions, bond-angle restrictions and so on [13,50–52]. Some of these constrained models were found to be unstable and changed significantly upon relaxation [17].

We have previously carried out calculations in the low density regime [38]. We worked in a density range of $0.923 \text{ g/cm}^3 - 1.6 \text{ g/cm}^3$. As a representative of this lower density regime in this paper, we have employed neutron diffraction data obtained for

¹ (M/N) are chosen with a ratio 0.01, with $M = 100$ and $N = 1$ for this work [26].

² A local-orbital density functional code using LDA with Ceperley-Alder exchange correlation [33].

³ RMC based applications for the structural refinement [37].

⁴ Jmol: an open-source Java viewer for chemical structures in 3D.

Table 1
Nomenclature and details of our models: Position of first minimum of RDF (r_{min}), average co-ordination number (n), percentage of sp^3 , sp^2 and sp and total CPU time for the simulation (T_0).

Models	$\rho = 3.50 \text{ (g/cm}^3\text{)}$			$\rho = 2.99 \text{ (g/cm}^3\text{)}$			$\rho = 2.44 \text{ (g/cm}^3\text{)}$			$\rho = 0.95 \text{ (g/cm}^3\text{)}$	
	F648	V160	S160	F648	V160	S160	F648	V160	S160	F648	V72 ^a
n	3.96	3.98	3.94	3.83	3.75	3.85	3.41	3.26	3.58	3.00	2.67
% of sp^3	96.00	97.50	93.75	82.70	75.00	85.00	42.00	26.87	58.13	10.80	—
% of sp^2	4.00	2.50	6.25	17.30	25.00	15.00	57.40	72.50	41.25	79.00	66.67
% of sp	—	—	—	—	—	—	0.60	0.63	0.62	9.60	33.33
T_0^b	28.12	100	—	30.73	100	—	23.58	100	—	—	—

^a At density 0.92 g/cm^3 [38].

^b CPU time for fixed number of total cores.

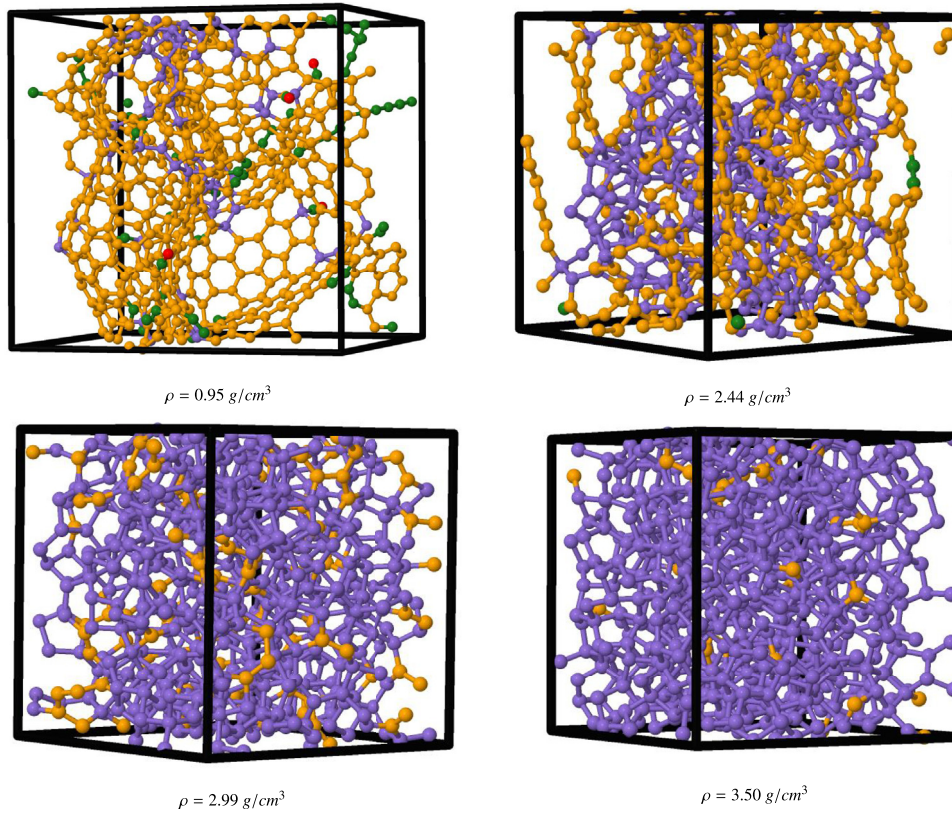


Fig. 1. (Color online) Visualization of the bonding in amorphous carbon for four different densities ρ . (F648): purple (sp^3), orange (sp^2), green (sp) and red (singly bonded). Periodic boundary condition were used, only atoms in reference cell are shown. Note the presence of amorphous graphene fragments with ring disorder at $\rho = 0.95 \text{ g/cm}^3$.

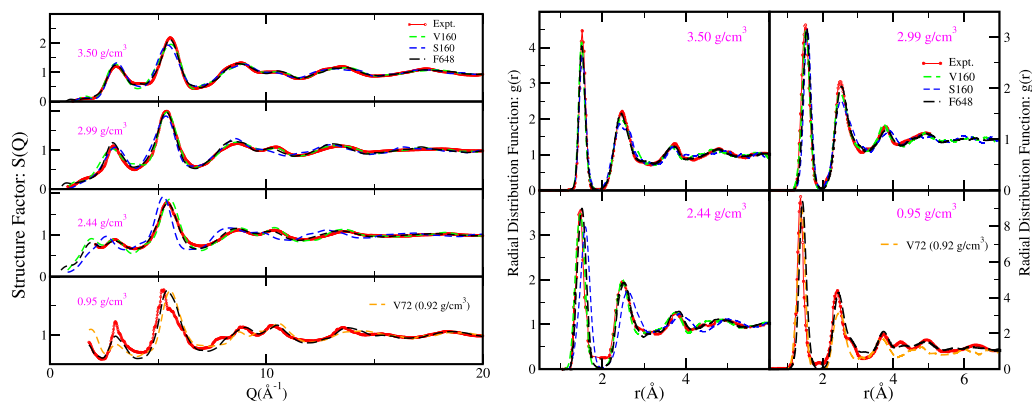


Fig. 2. (Color online) (Left panel) Structure factor for different models and their comparison with experiments (or WWW model for 3.50 g/cm^3). (Right panel) Radial distribution function of different models and their comparison with experiments. The experimental data are excerpted from previous literature [6,39–42].

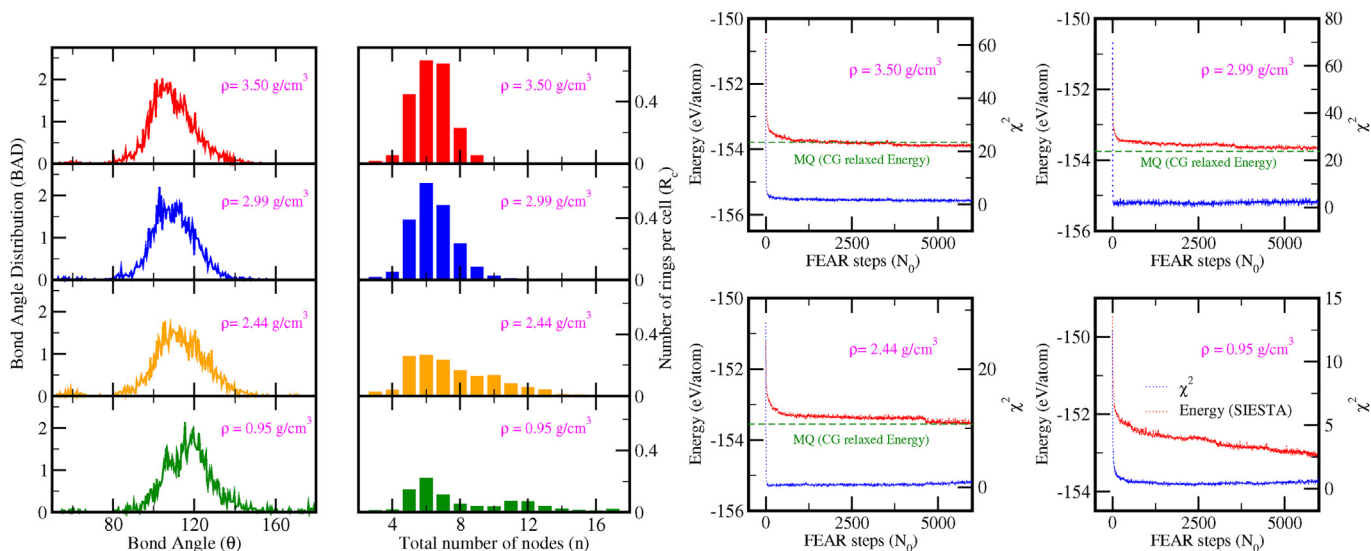


Fig. 3. (Color online) **Left panel**) Bond angle distribution (BAD) and Ring statistics of F648 models. **(Right panel)** Plot of total energy (SIESTA) per atom (red line, F648) and cost function (blue line, F648) (χ^2) versus number of FEAR steps (N_0). Final relaxed MQ energies are shown for comparison (green line, S160). (A colour version of this figure can be viewed online.)

silicon carbide-derived nanoporous carbon (SIC-CDC) [42] at a density 0.95 g/cm^3 as FEAR input. Our F648 model yields the most reliable picture of glassy carbon starting from random, a suitable minimum of SIESTA and without any bias (*ad hoc* constraints). The resulting model consists of obvious fragments of interconnected and warped amorphous graphene fragments (with sp^2 bonding, and ring disorder: hexagons, pentagons, heptagons and octagons). We have successfully reproduced the major RDF peaks for glassy carbon occurring at, 1.42 \AA , 2.46 \AA , 2.84 \AA and so on [2]. There is a slight deviation in the low Q range which was also observed in previous work [13,42] done with (> 3200 atoms), hinting that it is not a finite size artifact.

4.1. Bond angle distribution and ring statistics

Bond angle distribution (BAD) and ring statistics provide vital information about microstructure. In a typical RMC simulation with a perfect fit to experiment, an exaggerated peak near $\sim 60.0^\circ$ is observed in BAD [24]. Although, constraints have been employed [6] to avoid these unrealistic cases, FEAR achieves it without external bias. We report our results for BAD and ring statistics in Fig. 3.

At the highest density the BAD peak is close to the tetrahedral angle of 109.5° , with small deviation. At low densities the BAD peak is closer to 120.0° , indicating trigonal symmetry is dominant in these structures. It is reported that even with high sp^2 content BAD peak at low density is close to 117.0° [53].

We have shown in Fig. 3 that amorphous carbons mostly prefer 5–7 membered ring structures. This is also true for the high sp^2 concentration structures which further clarifies that these a-C structures are different from graphite (only 6 membered rings). A negligible fraction of smaller ring structures were also observed but these are less than MD and other calculations [6]. The ring statistics were evaluated with King's shortest path method [54] using ISAACS software [55].

4.2. Convergence and stability of FEAR carbon

In FEAR, we obtain low values of χ^2 in conjunction with a local

energy minimum.⁵ Our plot of the variation of total energy (E) and χ^2 is shown in Fig. 3. The results obtained shows that an initial structure is formed within few hundred FEAR steps. These states have more or less the same average energy and as we move along with FEAR steps these defects are removed, leading ultimately to a chemically realistic structure.

5. Electronic density of states

The concentration of sp , sp^2 and sp^3 sites strongly influences the electronic density of states (EDOS). As in the case of diamond, a-Carbon with high sp^3 is non-conducting. We have presented plots of the EDOS of our F648 models in Fig. 4, where we have also decomposed the total EDOS by sp^3 , sp^2 and sp contributions. We can clearly see that the sp^2 states for density 3.50 g/cm^3 act as a defect and leads to formation of a pseudo-gap [56]. Subsequently, a-Carbon models at lower density appear to be conducting as expected [43,57]. In Fig. 4 (Right panel) we show the plot of Inverse Participation Ratio (IPR) [58], IPR gives information about the spatial localization of electronic states. As seen in Fig. 4, the gap states for high density are highly localized while the lower two density have much more extended states.

6. Vibrational properties

The vibrational density of states (VDOS) provides crucial information about changes in local bonding environment which is very effective test for theoretical models [59] and offers a remarkably direct comparison between experiment and theory. It is well known that a-Carbon exhibits two major peaks in VDOS and Raman spectra; these occurring at: $\sim 1500 \text{ cm}^{-1}$ and $\sim 800 \text{ cm}^{-1}$ [41]. In contrast, several theoretical models show a single broad peak occurring roughly at $\sim 1100 \text{ cm}^{-1}$ [56,60].

We have also calculated the vibrational density of states (VDOS) of our four F648 models. The dynamical matrix was obtained by displacing each atom in 6-directions ($\pm x, \pm y, \pm z$) by a small

⁵ χ^2 measures goodness of fit between experimental and FEAR model [24–26].

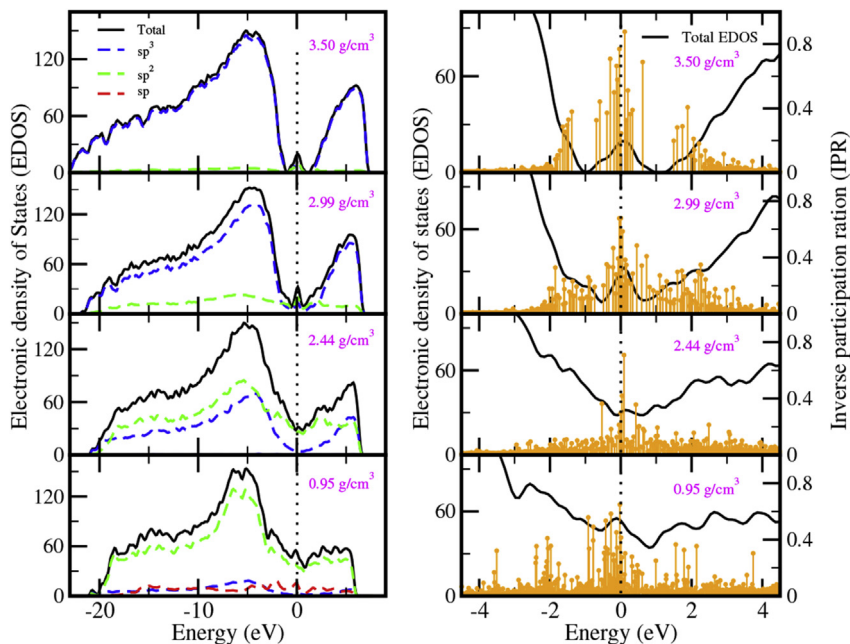


Fig. 4. (Color online) Plot of EDOS ($E_F = 0$ eV) for F648 models: (Left panel) black-solid (total EDOS), blue-dashed (sp^3 EDOS), green-dashed (sp^2 EDOS) and (green-dashed, sp EDOS). (Right panel) orange-drop lines (IPR) and black-solid (total EDOS). (A colour version of this figure can be viewed online.)

displacement of 0.015 \AA (see details [61]). Our VDOS plots for the four models are shown in Fig. 5.

Our results show reasonable agreement with the literature. There is distinct bifurcation seen in our F648 models as seen in several experiments. At 3.50 g/cm^3 , we compare our result with VDOS obtained for 216-WWW model [39]. We observed a slight shift for 2.99 g/cm^3 as compared to model at 3.50 g/cm^3 . At 2.44 g/cm^3 , we have compared our results (sp^3 fraction 42.0%) with experimental data [59] obtained for amorphous carbon containing sp^3 fraction at $60\% \pm 10\%$, we have a qualitative match with the

experimental finding. The position of two peaks and their relative intensity is reported to slightly differ for different incident energies and sp^3 fraction [59,63].

At low density 0.95 g/cm^3 , our model resembles distorted graphene structures (see Fig. 1). We have compared our results with 2D a-graphene result of Li and Drabold [62]. The plots bear a remarkable similarity, most notably the peak occurring at $\sim 700 \text{ cm}^{-1}$ and $\sim 1400 \text{ cm}^{-1}$. This is surprising in view of significantly different topology (one is 3-D, the other one 2-D!). We have also computed the inverse participation ratio (IPR) for our F648

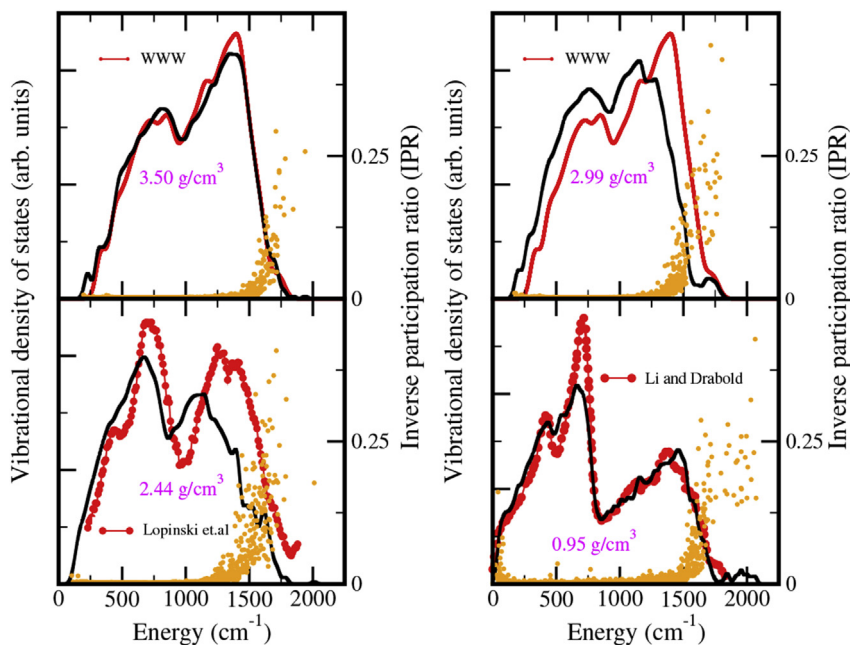


Fig. 5. (Color online) Plot of Vibrational density of states (VDOS) (black line, F648), comparison with previous literatures (red dots and lines) [39,59,62] and Inverse participation ratio (IPR) (orange dots) for F648 models. (A colour version of this figure can be viewed online.)

models. IPR, gives localization of these vibrational modes [38,61]. Our result for IPR shows that vibrational modes are extended at the low frequency regime and localized modes are only observed at a higher frequency than $\sim 1500\text{cm}^{-1}$, which are likely to be localized stretching modes [38,60].

7. Conclusions

We have used a *uniform approach* to model a-Carbon using FEAR at various densities. We have used method FEAR efficiency to obtain large size (648 atom) “*ab initio*” models. The inclusion of *ab initio* interactions not only guides us towards a chemically correct structures, it directly helps us to avoid chemically unphysical structures. A typical RMC based calculation fails to accurately model amorphous systems. In our experience, FEAR yields a *lower DFT energy* and takes far less computer time to converge compared to MQ with identical interactions.

We have established a set of accurate *ab initio* models for amorphous carbon that we hope will serve as a benchmark for future modeling studies.

Data availability

The coordinates of the four relaxed FEAR (648 atoms) models and of melt quench models prepared during this study are available from corresponding authors upon request.

Acknowledgment

The authors are thankful to the NSF under grant numbers DMR 1506836 and DMR 1507670. We thank Dr. Ronald L. Cappelletti for many helpful conversations, and indeed for motivating the entire study. We acknowledge the financial support from the Condensed Matter and Surface Science (CMSS) at Ohio University. We also acknowledge computing time provided by the Ohio Supercomputer Center. We also thank NVIDIA Corporation for donating a Tesla K40 GPU which was used in some of these computations.

References

- [1] J. Robertson, Diamond-like amorphous carbon, *Mater. Sci. Eng. R* 37 (2002) 129–281.
- [2] S.F. Parker, S. Imberti, S. Callear, P. Albers, Structural and spectroscopic studies of a commercial glassy carbon, *Chem. Phys.* 427 (2013) 44–48.
- [3] D.R. McKenzie, Tetrahedral bonding in amorphous carbon, *Rep. Prog. Phys.* 59 (1995) 1611–1664.
- [4] D.A. Drabold, P.A. Fedders, M. P. Grumbach, Gap formation and defect states in tetrahedral amorphous carbon, *Phys. Rev.* B545480–5484.
- [5] L. Li, M. Xu, W. Song, A. Ovcharenko, G. Zhang, D. Jia, The effect of empirical potential functions on modeling of amorphous carbon using molecular dynamics method, *App. Surf. Sci.* 286 (2013) 287–297.
- [6] G. Opletal, T.C. Petersen, D.G. McCulloch, I.K. Snook, I. Yarovsky, The structure of disordered carbon solids studied using a hybrid reverse monte carlo algorithm, *J. Phys. Condens. Matter* 17 (2005) 2605–2616.
- [7] D. R. McKenzie, D. Muller, B. A. Pailthorpe, Compressive-stress-induced formation of thin-film tetrahedral amorphous carbon, *Phys. Rev. Lett.* 67 773–776.
- [8] P. J. Fallon, V. S. Veerasamy, C. A. Davis, J. Robertson, G. A. J. Amaratunga, W. I. Milne, J. Koskinen, Properties of filtered-ion-beam-deposited diamondlike carbon as a function of ion energy, *Phys. Rev.* B484777–4782.
- [9] D. Mildner, J. Carpenter, On the short range atomic structure of non-crystalline carbon, *J. Non-Cryst. Solids* 47 (1982) 391–402.
- [10] D.A. Drabold, Topics in the theory of amorphous materials, *Eur. Phys. J. B* 68 (2009) 1–21.
- [11] R.L. McGreevy, L. Pusztai, Reverse monte carlo simulation: a new technique for the determination of disordered structures, *Mol. Simul* 1 (1988) 359–367.
- [12] P. Biswas, R. Atta-Fynn, D.A. Drabold, Reverse monte carlo modeling of amorphous silicon, *Phys. Rev. B* 69 (2004), 195207 (1–5).
- [13] B. O'Malley, I. Snook, D. McCulloch, Reverse monte carlo analysis of the structure of glassy carbon using electron-microscopy data, *Phys. Rev. B* 57 (1998) 14148–14157.
- [14] D.A. Keen, M.T. Dove, Local structures of amorphous and crystalline phases of silica, *sio2*, by neutron total scattering, *J. Phys. Condens. Matter* 11 (1999) 9263–9273.
- [15] V. Gereben, L. Pusztai, Structure of amorphous semiconductors: reverse monte carlo studies on a-c, a-si, and a-ge, *Phys. Rev. B* 50 (1994) 14136–14143.
- [16] G. Opletal, T.C. Petersen, A.S. Barnard, S.P. Russo, On reverse monte carlo constraints and model reproduction, *J. Comput. Chem.* 38 (2017) 1547–1551.
- [17] S.K. Jain, R.J.M. Pellenq, J.P. Pikunic, K.E. Gubbins, Molecular modeling of porous carbons using the hybrid reverse monte carlo method, *Langmuir* 22 (2006) 9942–9948.
- [18] J.K. Walters, K.W.R. Gilkes, J.D. Wicks, R.J. Newport, A new approach to modelling tetrahedral amorphous carbon, *J. Phys. Condens. Matter* 9 (1997) 457–463.
- [19] S. Hosokawa, W.C. Pilgrim, J.F. Berar, S. Kohara, Anomalous x-ray scattering studies on semiconducting and metallic glasses, *Eur. Phys. J. Spec. Top.* 208 (2012) 291–304.
- [20] S.J. Gurman, R.L. McGreevy, Reverse monte carlo simulation for the analysis of exafs data, *J. Phys. Condens. Matter* 2 (1990) 9463–9473.
- [21] M.G. Tucker, D.A. Keen, M.T. Dove, K. Trachenko, Refinement of the siosi bond angle distribution in vitreous silica, *J. Phys. Condens. Matter* 17 (2005) 67–75.
- [22] P. Biswas, D.N. Tafen, D.A. Drabold, Experimentally constrained molecular relaxation: the case of glassy *gese2*, *Phys. Rev. B* 71 (2005), 054204 (1–5).
- [23] G. Opletal, T. Petersen, B. Omalley, I. Snook, D.G. McCulloch, N.A. Marks, I. Yarovsky, Hybrid approach for generating realistic amorphous carbon structure using metropolis and reverse monte carlo, *Mol. Sim.* 28 (2002) 927–938.
- [24] A. Pandey, P. Biswas, D.A. Drabold, Inversion of diffraction data for amorphous materials, *Sci. Rep.* 6 (2016), 33731 (1–8).
- [25] A. Pandey, P. Biswas, D.A. Drabold, Force-enhanced atomic refinement: structural modeling with interatomic forces in a reverse monte carlo approach applied to amorphous *si* and *sio2*, *Phys. Rev. B* 92 (2015), 155205 (1–8).
- [26] A. Pandey, P. Biswas, B. Bhattarai, D.A. Drabold, Realistic inversion of diffraction data for an amorphous solid: the case of amorphous silicon, *Phys. Rev. B* 94 (2016), 235208 (1–8).
- [27] K. Prasai, P. Biswas, D.A. Drabold, Electronically designed amorphous carbon and silicon, *Phys. Status Solidi* 213 (2016) 1653–1660.
- [28] M.J. Cliffe, A.P. Bartok, R.N. Kerber, C.P. Grey, G. Csanyi, A.L. Goodwin, Structural simplicity as a restraint on the structure of amorphous silicon, *Phys. Rev. B* 95 (2017), 224108 (1–6).
- [29] M.J. Cliffe, M.T. Dove, D.A. Drabold, A.L. Goodwin, Structure determination of disordered materials from diffraction data, *Phys. Rev. Lett.* 104 (2010), 125501 (1–4).
- [30] J. Tersoff, Empirical interatomic potential for carbon, with applications to amorphous carbon, *Phys. Rev. Lett.* 61 (1988) 2879–2882.
- [31] N.A. Marks, Generalizing the environment-dependent interaction potential for carbon, *Phys. Rev. B* 63 (2000), 035401 (1–7).
- [32] C. Mathioudakis, G. Kopidakis, P.C. Kelires, C.Z. Wang, K.M. Ho, Physical trends in amorphous carbon: a tight-binding molecular-dynamics study, *Phys. Rev. B* 70 (2004), 125202 (1–10).
- [33] J.M. Soler, E. Artacho, J.D. Gale, A. Garcia, J. Junquera, P. Ordejon, D. Sanchez-Portal, The siesta method for *ab initio* order-n materials simulation, *J. Phys. Condens. Matter* 14 (2002) 2745–2779.
- [34] G. Kresse, J. Furthmuller, Efficient iterative schemes for *ab initio* total-energy calculations using a plane-wave basis set, *Phys. Rev. B* 54 (1996) 11169–11186.
- [35] G. Kresse, D. Joubert, From ultrasoft pseudopotentials to the projector augmented-wave method, *Phys. Rev. B* 59 (1999) 1758–1775.
- [36] P.E. Blochl, Projector augmented-wave method, *Phys. Rev. B* 50 (1994) 17953–17979.
- [37] M.G. Tucker, D.A. Keen, M.T. Dove, A.L. Goodwin, Q. Hui, Rmcprofile: reverse monte carlo for polycrystalline materials, *J. Phys. Condens. Matter* 19 (2007), 335218 (1–16).
- [38] B. Bhattarai, D.A. Drabold, Amorphous carbon at low densities: an *ab initio* study, *Carbon* 115 (2017) 532–538.
- [39] B. Djordjevic, M. Thorpe, F. Wooten, Computer model of tetrahedral amorphous diamond, *Phys. Rev. B* 52 (1995) 5685–5689.
- [40] K.W.R. Gilkes, P.H. Gaskell, J. Robertson, Comparison of neutron-scattering data for tetrahedral amorphous carbon with structural models, *Phys. Rev. B* 51 (1995) 12303–12312.
- [41] F. Li, J. Lannin, Radial distribution function of amorphous carbon, *Phys. Rev. Lett.* 65 (1990) 1905–1908.
- [42] A.H. Farmahini, G. Opletal, S.K. Bhatia, Structural modelling of silicon carbide-derived nanoporous carbon by hybrid reverse monte carlo simulation, *J. Phys. Chem. C* 117 (2013) 14081–14094.
- [43] D.G. McCulloch, D. McKenzie, C. Goringe, *Ab initio* simulations of the structure of amorphous carbon, *Phys. Rev. B* 61 (2000) 2349–2355.
- [44] A.C. Ferrari, A. Libassi, B.K. Tanner, V. Stolojan, J. Yuan, L.M. Brown, S.E. Rodil, B. Kleinsorge, J. Robertson, Density, *sp3* fraction, and cross-sectional structure of amorphous carbon films determined by x-ray reflectivity and electron energy-loss spectroscopy, *Phys. Rev. B* 62 (2000) 11089–11103.
- [45] P.J. Fallon, V.S. Veerasamy, C.A. Davis, J. Robertson, G.A.J. Amaratunga, W.I. Milne, J. Koskinen, Properties of filtered-ion-beam-deposited diamondlike carbon as a function of ion energy, *Phys. Rev. B* 48 (1993) 4777–4782.
- [46] F. Wooten, K. Winer, D. Weaire, Computer generation of structural models of amorphous *si* and *ge*, *Phys. Rev. Lett.* 54 (1985) 1392–1395.
- [47] D.N. Tafen, D.A. Drabold, Realistic models of binary glasses from models of

- tetrahedral amorphous semiconductors, *Phys. Rev. B* 68 (2003), 165208 (1–5).
- [48] C. Wang, K. Ho, Structural trends in amorphous carbon, *Phys. Rev. B* 50 (1994) 12429–12436.
- [49] A.H. Farmahini, S.K. Bhatia, Hybrid reverse monte carlo simulation of amorphous carbon: distinguishing between competing structures obtained using different modeling protocols, *Carbon* 83 (2015) 53–70.
- [50] T. Petersen, I. Yarovsky, I. Snook, D.G. McCulloch, G. Opletal, Structural analysis of carbonaceous solids using an adapted reverse monte carlo algorithm, *Carbon* 41 (2003) 2403–2411.
- [51] P. Zetterstrom, S. Urbonaite, F. Lindberg, R.G. Delaplane, J. Leis, G. Svensson, Reverse monte carlo studies of nanoporous carbon from tic, *J. Phys. Condens. Matter* 17 (2005) 3509–3524.
- [52] J. Pikunic, C. Clinard, N. Cohaut, K.E. Gubbins, J.-M. Guet, R.-M. Pellenq, I. Rannou, J.-N. Rouzaud, Structural modeling of porous carbons: constrained reverse monte carlo method, *Langmuir* 19 (2003) 8565–8582.
- [53] D. Beeman, J. Silverman, R. Lynds, M.R. Anderson, Modeling studies of amorphous carbon, *Phys. Rev. B* 30 (1984) 870–875.
- [54] S. King, Ring configurations in a random network model of vitreous silica, *Nature* 213 (1967) 1112–1113.
- [55] S. Roux, V. Petkov, Isaacs interactive structure analysis of amorphous and crystalline systems, *J. Appl. Cryst* 43 (2010) 181–185.
- [56] D.A. Drabold, P.A. Fedders, P. Stumm, Theory of diamondlike amorphous carbon, *Phys. Rev. B* 49 (1994) 16415–16422.
- [57] J. Robertson, E. O'Reilly, Electronic and atomic structure of amorphous carbon, *Phys. Rev. B* 35 (1987) 2946–2957.
- [58] C. Chen, J. Robertson, Nature of disorder and localization in amorphous carbon, *J. Non-Cryst. Solids* 227–230 (1998) 602–606.
- [59] G.P. Lopinski, V.I. Merkulov, J.S. Lanin, Vibrational states of tetrahedral amorphous carbon, *Appl. Phys. Lett.* 69 (1996) 3348–3350.
- [60] C. Wang, K. Ho, Structure, dynamics, and electronic properties of diamondlike amorphous carbon, *Phys. Rev. Lett.* 71 (1993) 1184–1187.
- [61] B. Bhattarai, D.A. Drabold, Vibrations in amorphous silica, *J. Non-Cryst. Solids* 439 (2016) 6–14.
- [62] Y. Li, D.A. Drabold, Symmetry breaking and low energy conformational fluctuations in amorphous graphene, *Phys. Status Solidi B* 250 (2013) 1012–1019.
- [63] P. Papanek, W.A. Kamitakahara, P. Zhou, J.E. Fischer, Neutron scattering studies of disordered carbon anode materials, *J. Phys. Condens. Matter* 13 (2001) 8287–8301.